Level-Crossing Determination of the $(6s6p)\,^3P_1$ hfs of Hg^{203} †

O. Redi
Palmer Physical Laboratory, Princeton University, Princeton, New Jersey 08540
and
H. H. Stroke ‡
Department of Physics, New York University, New York, New York 10453
(Received 2 January 1970)

The level-crossing technique has been used to measure the hyperfine structure of 47-day Hg^{203} and to remeasure the g_J value of Hg^{199} in the $(6s6p)\,^3P_1$ atomic state. The results, corrected for second-order perturbations arising from other fine-structure levels of the configuration, are $A = 4991.35(3)$ MHz, $B = -249.2(3)$ MHz, $g_J = 1.486\,110(9)$, and $A(Hg^{203})/A(Hg^{199}) = 0.338\,301(2)$. With these values, we calculate the nuclear moments $\mu = 0.856(9)\mu_N$ and $Q = 0.46(4)$ b. The value of μ includes a diamagnetic correction but not the calculated effect of the Hg^{199}-Hg^{203} hfs anomaly, $^{203}\Delta^{199} \approx -0.91\%$. The error brackets for μ and the hfs interaction constants allow for a hfs anomaly of $\pm 1\%$. The value of Q does not include the Sternheimer correction. Formulas are given for the dependence on geometry and polarization of level-crossing signals, and a method of correction for asymmetric line shapes is described. The influence of variation, over a large range, of B/A on the magnetic field positions of the level crossings for $J = 1$ has been studied. For $A = 0$ and neglecting the g_I term in the Hamiltonian, the energy displacement from the "center of gravity" and the magnetic field position of the single level crossing are shown to be $\sigma_c = -A/2$, and $H_c = (2I+1)\,|A|/2\mu_B g_J$, respectively.

I. INTRODUCTION

The hyperfine structure of atomic states of the stable and radioactive isotopes of mercury has been studied particularly intensively in the past decade as part of a systematic nuclear structure study of $_{80}$Hg and $_{81}$Tl.[1-3] Measurements of the atomic spectra can serve to give information about the nuclear spin and multipole moments as well as about the nuclear charge and magnetization distributions. The latter, which manifests itself through the hyperfine structure anomaly, requires a precise determination of the magnetic dipole interaction constants. Toward this end level-crossing and double-resonance experiments have been performed[1,2,4,5] in the $(6s6p)\,^3P_1$ state of $Hg^{193*,195,195*,197,197*,199,201}$. Work on Hg^{193} is still in progress.[5] The present experiment extends these measurements to 47-day Hg^{203}.

The hfs anomaly arises from the difference in the interaction of the nuclear magnetization of finite extent with an inhomogeneous and a homogeneous magnetic field. The hfs interaction of a penetrating electron corresponds to the former situation, while the magnetic interaction in nuclear resonance experiments corresponds to the latter. The precise nuclear magnetic resonance experiments[1,2,6] for $Hg^{195,197,199,201}$ have been performed by optical pumping techniques, thereby providing the data required for hfs anomaly determinations.

The optical spectroscopic experiments on Hg^{203} reported earlier[7] gave a value of the nuclear spin, isotope shift, magnetic moment (to $\pm 2\%$) and a rough value of the quadrupole moment. The results of the level-crossing experiment are consistent with the earlier results. This completes a precise determination of the Hg^{203} hfs and the nuclear moments derived from it. The present results also permit an improved determination of the isotope shift[8] when combined with the optical data.

The level-crossing method of atomic spectroscopy of Franken, Colgrove, Lewis, and Sands[9] was first applied to hfs studies by Hirsch.[10] The method involves the observation of changes in the angular distribution of resonance fluorescence from an atomic vapor as a function of applied magnetic field. The changes observed occur when two particular excited-state magnetic sublevels become degenerate ("cross"). A corrected calculation for the angular distribution of the resonance fluorescence has been given by us recently.[11] From the measurement of the magnetic fields at which the level crossings occur, hfs interaction constants can be calculated in units of $\mu_B g_J$, where μ_B is the Bohr magneton and g_J is the electronic g factor. An accurate determination may require taking into account the perturbations arising from neighboring fine-

structure levels.

The required g_J value for the $^3P_1$ state of Hg was redetermined from a level-crossing experiment on Hg^{199} for which the hfs is known from an independent double-resonance experiment. The observation of the level crossings of Hg^{203} and Hg^{199} in the same experimental situation furthermore allows a more direct determination of the ratio of the hfs interaction constants of the isotopes. This can have importance in the hfs anomaly determination.

II. THEORY

A. Resonant Scattering near Level Crossings

The theory of resonant scattering in the case of crossing excited states has been discussed by Weisskopf[12] and Breit[13] and more recently by Franken[14] (and in a corrected version by us[11]), Rose and Carovillano, [15] Lassila, [16] and Wieder and Eck. [17] The last two references give a general derivation which includes both the "crossing" and the "anticrossing" effects. Only the former is of importance in this work.

The resonant scattering process under consideration is that of the $^1S_0 - {}^3P_1$ 2537-Å transition (see Fig. 1). The Doppler linewidth of the light source and of the absorption line is approximately 800 times greater than the natural linewidth: Therefore, the illumination can be considered constant over the natural linewidth. In our experiment we observe the change in the angular distribution of the scattered light as the magnetic field is varied by monitoring the intensity of the radiation in one fixed direction.

The magnetic substates of the $^1S_0$ and the $^3P_1$ states will be labeled by m and μ, respectively. In the region of the external magnetic field where the crossing occurs for the substates μ and μ', the expression for the scattered light intensity I is

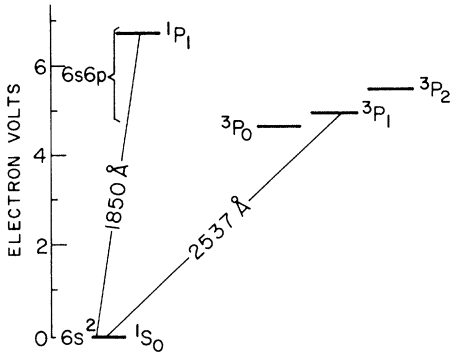

FIG. 1. Atomic energy levels of mercury below 7 eV.

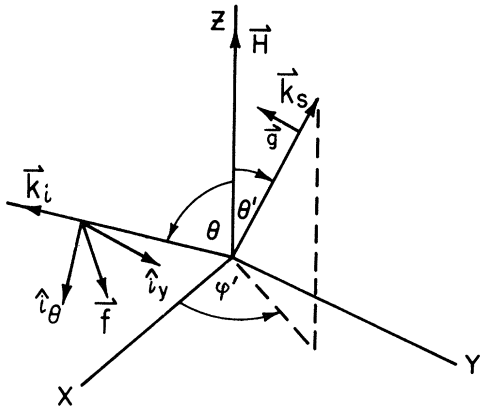

FIG. 2. Coordinate system and propagation and polarization vectors used in the calculation of $A_{\mu,\mu'}$. The vector $\vec{k}_i$ lies in the x-z plane.

$$I \propto R_0 + \frac{A_{\mu,\mu'} + A^*_{\mu,\mu'}}{1+x^2} - \frac{ix(A_{\mu,\mu'} - A^*_{\mu,\mu'})}{1+x^2}, \quad (1)$$

where $x \equiv \tau(E_\mu - E_{\mu'})/\hbar$. (We emphasize the minus sign in front of ix. An incorrect sign has been quoted in most publications on level-crossing experiments.) E_μ, $E_{\mu'}$ denote the energies of the excited substates μ and μ', and τ is the excited-state mean life. R_0, which represents the portion of the light scattered independently of the difference of E_μ and $E_{\mu'}$, is given by

$$R_0 = \sum_{m,m',\mu} |f_{\mu m}|^2 |g_{m'\mu}|^2 . \quad (2)$$

The observable change in the angular distribution of the scattered radiation at a level crossing is implicit in the last two terms of (1) where we defined

$$A_{\mu,\mu'} \equiv \sum_{m,m'} f_{\mu m} f^*_{\mu' m} g^*_{m'\mu'} g_{m'\mu} . \quad (3)$$

The quantities f_{ij} and g_{ij} are the electric dipole matrix elements $\langle i|\vec{f}\cdot\vec{r}|j\rangle$ and $\langle i|\vec{g}\cdot\vec{r}|j\rangle$. The polarization vectors of the incident and scattered light are given by $\vec{f}$ and $\vec{g}$, and the electric dipole moment operator is $-e\vec{r}$.

We shall now obtain an explicit expression for $A_{\mu,\mu'}$ in terms of the wave vector $\vec{k}_i$ and polarization directions of the incident light, and the wave vector $\vec{k}_s$ of the scattered light. Because measurements are made to a precision of the order of one-twentieth of a linewidth, a sufficiently general knowledge of the dependence of $A_{\mu,\mu'}$ on these quantities, shown in Fig. 2, is required in order to understand and be able to correct for the effects on the observed line shape of possible deviations from the simple rectangular geometry. It can be

seen from (1) that if $A_{\mu,\mu'}$ is real, the line shape (scattered light intensity versus magnetic field H) is Lorentzian with a full width at half-maximum:

$$\Delta H = \left| dH/d(E_\mu - E_{\mu'}) \right| (2\hbar/\tau) \ . \tag{4}$$

[In our experiments, the variation of $A_{\mu\mu'}$ and $|dH/d(E_\mu - E_{\mu'})|$ with H over a linewidth can be neglected.] In general, however, $A_{\mu\mu'}$ may be complex, thereby producing an asymmetrical line shape. Our calculation of $A_{\mu,\mu'}$ will involve a summation over the polarization directions of the scattered light, since in our experiments no polarizers are used to observe it.

The magnetic field $\vec{H}$ defines the direction of the z axis. The x-z plane is defined by $\vec{k}_i$ and $\vec{H}$ so that the x component of $\vec{k}_i$ is positive.[18] In general, $\vec{k}_i$ is at an angle θ with respect to the z axis, and $\vec{k}_s$ is described by angles θ', φ' shown in Fig. 2. We therefore resolve the polarization vector:

$$\vec{f} = f_a \hat{i}_y + f_b \hat{i}_\theta = f_b \cos\theta \hat{i}_x + f_a \hat{i}_y - f_b \sin\theta \hat{i}_z \ , \tag{5}$$

where f_a and f_b are, in general, complex numbers. In terms of spherical tensor notation we have

$$\vec{f} \circ \vec{r} = -f_1 r_{-1} + f_0 r_0 - f_{-1} r_1 \ , \tag{6}$$

where $f_1 = -(1/\sqrt{2})(f_b \cos\theta + i f_a)$, $f_0 = -f_b \sin\theta$,

$$f_{-1} = (1/\sqrt{2})(f_b \cos\theta - i f_a) \ ,$$

$$r_1 = -(1/\sqrt{2})(x + iy), \quad r_0 = z, \quad r_{-1} = (1/\sqrt{2})(x - iy) .$$

From electric dipole selection rules, a nonzero value of $A_{\mu,\mu'}$ can be obtained only if μ and μ' differ by 0, 1, or 2. The first possibility does not occur since levels of the same μ value do not cross. Only the case $\Delta\mu = 2$ is of interest here, since for the particular geometry used $\Delta\mu = 1$ crossings are not observable, as shown in Appendix A. For the case of crossings of hyperfine magnetic substates we associate μ and m with the appropriate m_F, where F denotes the total angular momentum quantum number. The explicit expression[18] for (3) that applies in the case $\mu = m_F + 1$, $\mu' = m_F - 1$, becomes, therefore,

$$A_{\mu,\mu'}(\mu > \mu') = A_{m_F+1,\, m_F-1} = \left| \langle \alpha', m_F - 1 | r_{-1} | \gamma, m_F \rangle \right|^2$$

$$\times \left| \langle \alpha, m_F + 1 | r_1 | \gamma, m_F \rangle \right|^2 (2\pi/15)^{1/2} Y_2^2(\theta', \varphi')$$

$$\times [\,|f_a|^2 - |f_b|^2 \cos^2\theta + i(f_a f_b^* + f_a^* f_b)\cos\theta\,] \ . \tag{7}$$

The quantities α and α' label all the remaining quantum numbers of the two $^3P_1$ crossing magnetic sublevels, and γ, those of the $^1S_0$ ground state.

The experiment is designed for the rectangular geometry $\theta = \theta' = \varphi' = 90°$, $f_a = 1$, $f_b = 0$, for which $A_{\mu\mu'}$ is seen to be real. $A_{\mu\mu'}$ becomes complex (i) if $\varphi' \neq 90°$, (ii) if $\theta \neq 90°$, and if at the same time $f_a f_b^* + f_a^* f_b \neq 0$. Equation (7) shows that the sign of $\mathrm{Im}(A_{\mu\mu'})$ reverses if the direction of the magnetic field is reversed ($\theta \to \pi - \theta$, $\theta' \to \pi - \theta'$, $\varphi' \to 2\pi - \varphi'$). Thus, any errors that may result from line asymmetry caused by possible optical misalignment of the apparatus can be corrected by making measurements with both senses of the applied magnetic field and then taking the average of the results.

Equation (7) is also used for calculating the strengths of the level-crossing signals, and an example is given in Appendix B. The calculations will be compared to experimental results in Sec. III B.

B. hfs and Second-Order Corrections

The Hamiltonian[19,20] which was used to calculate the Hg $(6s6p)\ ^3P_1$-state magnetic dipole ($k = 1$) and electric quadrupole ($k = 2$) hyperfine and magnetic field first-order interaction energies and the second-order perturbations caused by the other states of the $6s6p$ configuration is

$$\mathcal{H} = \sum_i (T_e^{(1)}(i) \cdot T_n^{(1)} + T_e^{(2)}(i) \cdot T_n^{(2)}) + \mu_B (g_s \vec{S} + g_L \vec{L} + g_I \vec{I}) \cdot \vec{H} \ . \tag{8}$$

In this expression, $T_e^{(k)}(i)$ and $T_n^{(k)}$ are tensor operators of rank k operating in the space of the coordinates of the ith valence electron and the nucleons, respectively, and $\vec{S}$, $\vec{L}$, and $\vec{I}$ are the total electronic spin, the total electronic orbital, and nuclear angular momentum vectors.

Lurio, Mandel, and Novick[20] have calculated expressions for the matrix elements of $\mathcal{H}$ in the F, m_F representation, diagonal and off-diagonal in the fine-structure states of an sl configuration. The diagonal elements serve to define the hfs interaction constants A and B and the g_J value as they are defined usually in theoretical treatments[21] that omit the off-diagonal elements. The complete matrix for the configuration can be transformed, using a theorem from perturbation theory[22] (known as the Van Vleck transformation), to one for which the off-diagonal elements are nearly zero. The eigenvalues of the resulting matrices for each fine-structure state give the energies with second-order Zeeman, hyperfine, and cross Zeeman-hyperfine corrections.

The second-order corrections were important in the analysis of the Hg^{199} and Hg^{203} level-crossing data as discussed in Secs. III B3 and III B4. For the purposes of preliminary data analysis, as well as for a study of the general behavior of

the level-crossing field values as a function of the hyperfine interaction constants, the second-order corrections can be neglected. In this case, the Hamiltonian can be rewritten in terms of $\vec{I}$ and the total electronic angular momentum $\vec{J}$ as[21]

$$\mathcal{H}' = A'\vec{I}\cdot\vec{J} + B'Q_{op} + \mu_B(g_J'\vec{J} + g_I\vec{I})\cdot\vec{H}\,, \qquad (9)$$

where A' and B' are the uncorrected interaction constants, g_J' is the uncorrected g_J value, and

$$Q_{op} \equiv [3(\vec{I}\cdot\vec{J})^2 + (\tfrac{3}{2})(\vec{I}\cdot\vec{J}) - \vec{I}^2\vec{J}^2]\,/[2I(2I-1)J(2J-1)]$$

C. Level Crossings with $\Delta m_F = 2$ for a $J = 1$ State

For an atom with $J = 1$ that has a normal ordering of zero-field hfs states we have the following characteristics for the $H \neq 0$, $\Delta m_F = 2$ level crossings. There is one crossing (the "main" crossing) that involves a $F = I + 1$, $m_F = \mp(I+1)$ state and a "F" $= I$, $m_F = \mp(I-1)$ state, where the upper and lower signs refer to a positive and negative A value. For $I > 1$ there are additional level crossings which occur among levels with "F" $= I$ and "m_J" $= 0$ (quantum numbers at the low- and high-field limits, respectively). These crossings ("foldover" crossings) occur as the levels undergo a complete reversal of ordering. The above level crossings can be seen on the energy level diagrams for Hg^{203} ($I = \frac{5}{2}$) shown in Figs. 3 and 4. The influence of the variation of B/A on the positions of these level crossings is shown in Fig. 5. The position of the main crossing can be seen to be very insensitive to the variation of B/A when compared to the foldover crossings. The number of foldover crossings varies, depending on the value of B/A, from a maximum of $2I$-2 to a minimum of $I - \frac{3}{2}$ or $I - 2$ for $2I$ odd and even, respectively. A third type of crossing is represented by the dotted curves in Fig. 5. These crossings arise when a reordering of the levels takes place in reaching the high-field pattern,

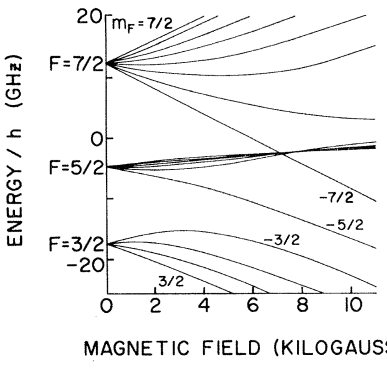

FIG. 3. Magnetic-field dependence of hfs energy levels of Hg^{203} ($I = \frac{5}{2}$) in the $^3P_1$ state.

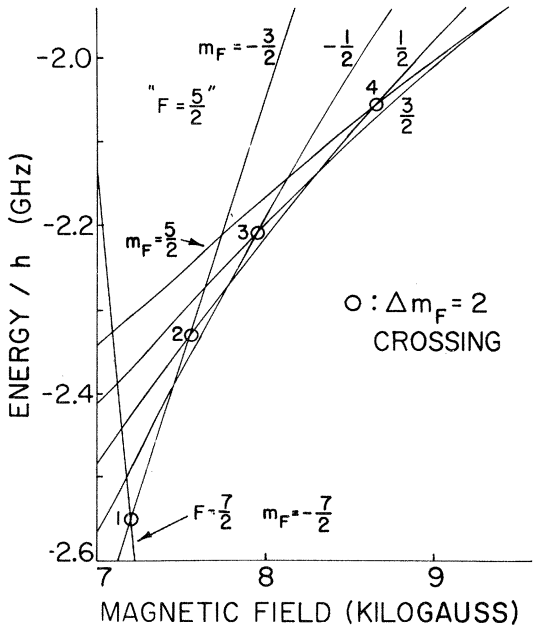

FIG. 4. Details of the Hg^{203} hyperfine energy level diagram (Fig. 3) in the level-crossing region. The main crossing and the foldover crossings are labeled No. 1 and Nos. 2, 3, and 4, respectively.

where for $m_J = 0$ the levels with equal $|m_F|$ are paired. The signal strengths of these crossings ($\propto A_{\mu\mu'}$) for a given B/A are lower than for those already mentioned. Only the crossing labeled

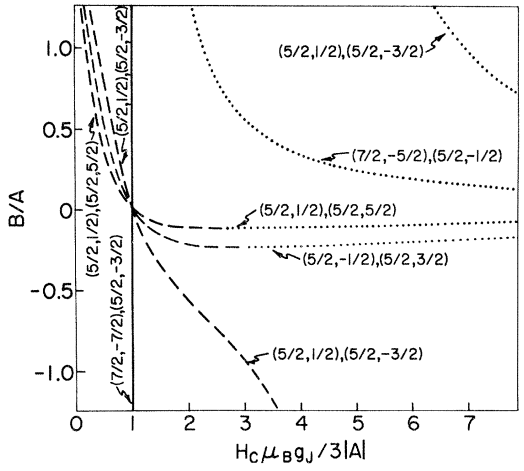

FIG. 5. Relationship, for $I = \frac{5}{2}$, between B/A and the level-crossing magnetic field values H_c given in units of $3|A|/\mu_B g_J$. The solid curve and the dashed curves correspond to the main and the foldover crossings, respectively. The dotted curves correspond to a third type of crossing discussed in the text. The given labels ("F", m_F), ("F'", m_F') are for $A > 0$. A diagram for $A < 0$ can be obtained by changing the signs of m_F.

$(\frac{7}{2}, -\frac{5}{2})$, $(\frac{5}{2}, -\frac{1}{2})$ in the region $B/A \gtrsim 1$ appears to be of value for level-crossing spectroscopy because of its strength and narrow linewidth:

$$h^{-1}\left|d(E_\mu - E_{\mu'})/dH\right| \geq 0.4\ \text{MHz/G}$$

for $B/A \geq 1$.

Above we have considered a normal ordering of zero-field hfs levels characterized by a small B/A. A diagram similar to Fig. 5 for a wide range of B/A for $I = \frac{5}{2}$ is given in Appendix C. The method of calculation is also given in this Appendix.

In Appendix C, it is shown that for $B = 0$, I arbitrary, and neglecting the g_I term in the Hamiltonian (and also the second-order corrections), all the level crossings occur for the same value of magnetic field:

$$H_c = (2I+1)\left|A\right|/2\mu_B g_J \qquad (10)$$

and at the same energy displacement from the "center of gravity":

$$\sigma_c = -A/2 \ . \qquad (11)$$

The characteristics discussed here are useful in searching for level crossings and in their identification as is shown below.

III. EXPERIMENT

A. Apparatus

Figure 6 is a diagram of the optical arrangement used for the level-crossing experiment. The source of 2537-Å resonance radiation was a Hg^{202} $(I = 0)$ electrodeless discharge lamp placed in the field of a small ("scanning") electromagnet.

The value of the magnetic field was set so as to shift the wavelength of one of the Zeeman components[2,23] of the Hg^{202} emission line to a value necessary to excite the crossing levels in either Hg^{203} or Hg^{199}. As can be seen from (7), for the

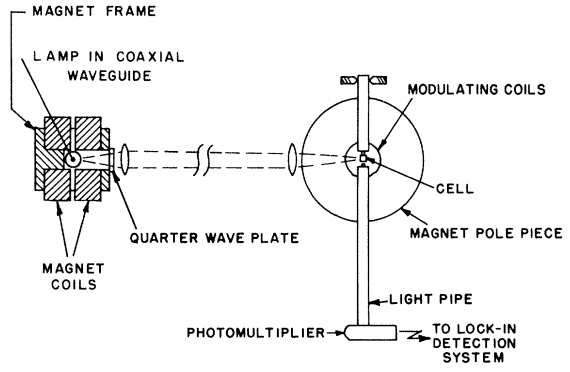

FIG. 6. Schematic diagram of the apparatus.

geometry used in this experiment only the component of the polarization vector f_a is effective in producing the $\Delta m_F = 2$ level-crossing signal. In order to maximize f_a at the wavelength of one of the σ Zeeman components, we used the circularly polarized light emitted in the direction of the magnetic field passed through a quartz quarter-wave plate. The light was focused onto the scattering cell by means of two quartz lenses.

The cell that contained the mercury vapor was supported inside a 2-in. gap of a 12-in. Harvey-Wells L-128 electromagnet. The scattered 2537-Å radiation reached the magnetically shielded RCA 1P28 photomultiplier through a light pipe. (The 1840-Å resonance radiation was not detected because of strong absorption at this wavelength by the photomultiplier envelope, a Vycor cell window, and the air.)

The light pipe was a glass tube coated on the inside with evaporated aluminum. Coils, 3 in. in diameter, were mounted on the pole faces to permit the modulation of the magnetic field and hence also of the scattered light intensity at the level-crossing field. The resulting modulated signal was detected with the use of a lock-in detector (Princeton Applied Research JB-5).

1. *Magnetometer*

The magnetic field at the scattering cell was measured by a proton magnetic-resonance (NMR) magnetometer in which was used a Rollin circuit[24] that incorporates a Gertsch FM-6 rf generator. The frequency of this unit is stabilized by a phase-lock to a crystal oscillator. The signal was displayed on an oscilloscope with a sweep frequency twice that of the magnetic field modulation. In this manner the line center was indicated by the coincidence of two identical resonance curves corresponding to successive half-cycles of the modulation frequency. In the magnetic field range used for the present experiments the signal-to-noise ratio for this magnetometer was sufficient to allow the detection of a magnetic field difference as low as about 7 mG.

The cylindrical NMR probe contained a 0.01 molal solution of $FeCl_3$ in H_2O for which the resonance frequency is equal to that of a spherical probe containing pure water except for a small correction[25] for bulk diamagnetism $\Delta = -0.7(3)\times 10^{-6}$. The proton resonance frequencies ν_p were converted to frequencies corresponding to $\mu_B H$ by the relation

$$h^{-1}\mu_B H = \nu_p\,(\mu_B/2\mu_p') = 328.7323\,(3)\nu_p \ . \qquad (12)$$

Here we have

$$\mu_B/\mu_p' = (1+\Delta)(\mu_B/\mu_p)_{H_2O,\ \text{sphere}} ,$$

with $(\mu_B/\mu_p)_{H_2O,\,\text{sphere}}$ from Ref. 26.

The small difference in the value of the magnetic field at the positions of the scattering cell and the NMR probe varies with the history of the magnetic field, and hence was remeasured for each level-crossing determination ("cell-to-probe correction").

The measurement of the cell-to-probe correction was made in a time sufficiently short ($\approx$ 3 sec) so that the unavoidable magnetic field variation caused by instabilities in the current from the Harvey-Wells HS 1365B power supply and in the magnet iron characteristics was less than 1 ppm. The required rapid field comparison was achieved with the use (i) of a mount for simple and accurate repositioning of the NMR probe, as shown in Fig. 7, and (ii) of the NMR circuit, the frequency of which was stable and unaffected by changes in capacitance that result from variations of the probe position.

2. *Light Source and Scattering Cells*

The electrodeless discharge lamp was made of a 7-mm-diam 10-cm-long quartz tube filled with 1 Torr of argon and 2 mg of 92% enriched Hg^{202}. The lamp was microwave excited and air cooled to reduce self-reversal.

The cubical cells, 1 cm on a side, were made from Beckman No. 46009 cells which consist of a U-shaped Vycor piece with a polished bottom and two fused silica windows. Each Beckman cell was shortened and a fused silica window with a 5-mm-diam appendage was fused on. The face of each cell through which the light entered was fitted with a mask to reduce scattering from its walls. Details of lamp and cell manufacture and radioactive sample transfer will be given in a subsequent paper on the optical spectrum of Hg^{203}.[8] The cell used in the Hg^{203} measurements was filled with approximately 4×10^{14} atoms of Hg^{203} produced in a nuclear reactor from Hg^{202} contained in natural Hg. After enrichment with the Argonne National Laboratory mass separator, a Hg^{203}-Hg^{202} ratio of the order of $\frac{1}{3}$ was obtained.[27] The sample contained a sufficient quantity of Hg^{199} and Hg^{201} for the observation of a level-crossing signal. Another cell of the same construction, filled with natural Hg, was used for some of the Hg^{199} measurements.

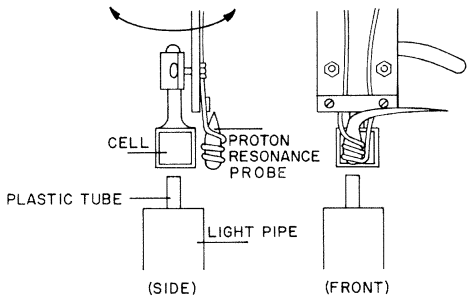

FIG. 7. Cell-NMR probe mount. The arrows indicate its movement during a measurement of the cell-to-probe correction.

B. Procedure and Results

The search problem for the Hg^{203} level crossings was minimized by the availability of the optical spectroscopic hfs and isotope shift data. These data were sufficiently accurate for the calculation of the required scanning field for the Hg^{202} lamp ($\approx$ 2000 G, σ^- component) and to narrow the possible magnetic field range for the expected level crossings. It is convenient to calculate approximate values of these two fields with the use of the relationships given by (10) and (11).

Four new level crossings were found in addition to the ones of the natural isotopes Hg^{199} and Hg^{201}. The assignment of the new level crossings to Hg^{203} was made on the basis of the selective sensitivity of the experiment for Hg by means of the wavelength of the resonance line and on the basis of the method of production, mass spectrographic enrichment, and half-life of the sample. Figure 8 shows typical recorder traces of the level-crossing signals. After allowing the sample to decay 128 days (2.7 half-lives) crossings Nos. 1, 2, and 3 could still be observed, but with relatively lower signal strength.

1. *Identification of Level Crossings*

For the rectangular geometry described above only $\Delta m_F = 2$ level crossings are observable (see Sec. II A). The possibility that $\Delta m_F = 1$ crossings were observed because of a small deviation from the rectangular geometry was checked by observing the signal as a function of the direction of polarization of the incident light. The level assignments for the observed $\Delta m_F = 2$ crossings and the determination of the hfs constants were made uniquely from the values of the level-crossing magnetic fields with the knowledge of the nuclear spin[7] $I = \frac{5}{2}$ and the sign of the nuclear magnetic moment,[7] and, of course, the appropriate atomic properties. The unique hfs determination was made by the use of the diagram in Appendix C to check which values (all values were considered) of A and B are consistent with the four experimental level-crossing fields. Energy-level diagrams displaying the four level crossings are shown in Figs. 3 and 4.

A further check on the interpretation of the level crossings is provided by the comparison of the

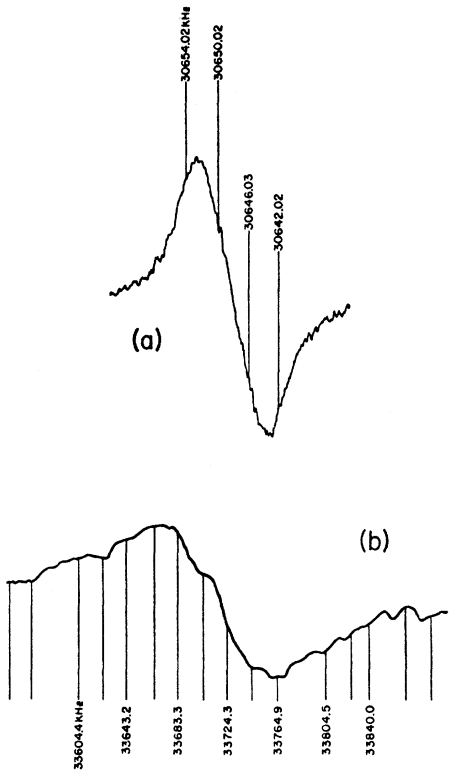

FIG. 8. Typical recorder tracings of the lock-in detector output for (a) level crossing No. 1 with a lock-in time constant $T=3$ sec and for (b) level crossing No. 3 with $T=10$ sec. The calibration of the magnetic field sweep is given by the NMR frequency markers. The amplitude of the 36-Hz field modulation was set for a maximum signal. The line centers are shifted because of the finite lock-in time constant.

theoretical and observed linewidths and relative strengths of the crossing signals. This is shown in Tables I and II.

We would like to point out that, because of the linewidths involved, our level-crossing data alone are not sufficient for an unambiguous simultaneous determination of the spin and the magnitudes and signs of the hfs interaction constants. This is illustrated by the results shown in Table III. However, the sign of the ratio A/B can be determined. In cases when Zeeman tuning of the lamp is used, the additional knowledge of this Zeeman field and of the isotope shift may provide the basis for selecting the correct set of I, A, and B. For example, the scanning fields on the Hg^{202} lamp required to maximize the main crossing signal in Hg^{203} for positive and negative A values are approximately 2000 G (σ^- component) and 400 G (σ^+ component), respectively. This method or the method given in Ref. 11 for determining the sign of A was not needed for Hg^{203}.

TABLE I. Experimental and theoretical Hg^{203} level-crossing linewidths. The theoretical values were calculated from (4) with $\tau=8.9(10)\times10^{-8}$ sec. This value of τ was obtained from a least-squares fit to the linewidth data. The deviation of this value of τ from the known value,[a] $1.18(2)\times10^{-7}$ sec, is probably due to residual gas pressure broadening. To a precision of better than one part in 10^6, no displacements of the crossing field are observed under the influence of either mercury-mercury, or mercury–foreign-gas collisions up to pressures of several Torr, or because of trapping of resonance radiation.[b] The cell temperature was 20–24 °C. The experimental linewidths were determined from the lock-in detector output curves using the relationships of Ref. c. Because of low signal strength, a determination of modulation broadening was not attempted for crossing No. 4.

Crossing No.	Experimental ΔH (G)	Theoretical ΔH (G)
1	1.3(2)	1.3
2	12(2)	9.6
3	17(5)	23.
4	>16 <55	47.

[a]J. P. Barrat, J. Phys. Radium 20, 541 (1959); 20, 633 (1959); 20, 657 (1959).

[b]J. Brossel and J. P. Faroux, Ecole Normale Supérieure, Paris, (private communication).

[c]H. Wahlquist, J. Chem. Phys. 35, 1708 (1961).

2. *Precision Measurements of Level Crossings*

Two procedures were used to determine the line center of the level-crossing signals to a precision of the order of $\frac{1}{20}$ of the width. The first one consisted in sweeping the magnetic field over the region of the level crossing while monitoring the NMR frequency. Curves were obtained with increasing and decreasing magnetic field sweeps and the results averaged in order to cancel the error that results from response lag time of the lock-in detector. Typical recorder tracings are shown in Fig. 8.

The second procedure, one that we used in most of the measurements, was essentially a point-by-

TABLE II. Experimental and theoretical amplitude ratios of the Hg^{203} level-crossing signals. The amplitudes measured with a lock-in detector are $S\propto A_{\mu\mu'}$, where $A_{\mu\mu'}$ is calculated from (7). In the analysis of the data, the relationship between the lock-in detector output amplitude and the field modulation amplitude given in Ref. a was used.

	Experimental	Theoretical
$S(1)/S(2)$	8.4(10)	9.1
$S(2)/S(3)$	1.8(2)	1.9
$S(3)/S(4)$	2.9(4)	3.2

[a]H. Wahlquist, J. Chem. Phys. 35, 1708 (1961).

TABLE III. Consistency of the Hg^{203} level-crossing data with various combinations of nuclear spin and hyperfine interaction constants. For fixed values of spin and signs of the interaction constants, the calculated[a] A' and B' were obtained by assigning the four observed crossings to the first four $\Delta m_F = 2$ crossings that are predicted to occur as the magnetic field is increased. The inclusion of the second-order corrections did not alter significantly the minimized values of χ^2 given in this table.

I	A' (MHz)	B' (MHz)	χ^2	
$\frac{1}{2}$				inconsistent with the four observed level crossings
$\frac{3}{2}$				
$\frac{5}{2}$	4990.88	−255.2	0.17	
$\frac{5}{2}$	−4991.48	238.5	0.27	
$\frac{7}{2}$	3743.33	−400.2	0.22	χ^2 fit
$\frac{7}{2}$	−3743.66	380.3	0.05	satisfactory
$\frac{9}{2}$	2994.78	−548.7	4.9	
$\frac{9}{2}$	−2994.99	526.7	3.3	
$\frac{11}{2}$	2495.74	−700.2	25	χ^2 fit
$\frac{11}{2}$	−2495.89	676.7	21	unsatisfactory

[a]Calculation performed with the HYPERFINE-4 computer program (see Ref. 30).

point one. This permitted us to take advantage of long time constants (30 sec) to average out noise without the associated problems of long-term drift for slow sweeps and distortion of the lock-in detector output for too rapid sweeps. Measurements of the lock-in detector output were made for periods of about 8 min for several constant values of the magnetic field around the level crossing. A few measurements were made at magnetic fields several linewidths higher and lower than the center in order to determine the background. After each new magnetic field setting, sufficient time was allowed for detector response lag time before making a measurement. We reduced the effects of long-term drifts resulting, for example, from a change in the lamp intensity by selecting a random sequence of magnetic fields around and far away from the level crossing. Figure 9 shows typical recorder tracings. The magnetic field was continuously monitored and corrected manually to within ±10 and ±25 mG for the main and other level crossings, respectively. This procedure allowed some improvement of the field stability over that which existed in the field-sweep runs.

For crossings Nos. 2, 3, and 4, high-modulation magnetic field amplitudes had to be used, and a detectable modulation of the scattered light was produced even when no level-crossing signal was present. This was assumed to arise from a shifting of the absorption lines of Hg^{203} and the stable Hg in the cell with respect to the incident-light wavelength. The slow change of the lock-in detector output as a function of magnetic field due to this effect can be seen in Figs. 8(b) and 9(b) as a difference in the background at the magnetic fields above and below the level crossing. This change of the background was taken into account in the determination of the line center by assuming that it is linear over the linewidth.

Two ways were used to avoid errors caused by asymmetric line shapes. The method of taking the average of measurements with both senses of the magnetic field was discussed in Sec. II A. The more common method consisted of an adjustment of the effective scattering angle φ' until an antisymmetric output curve was obtained from the lock-in detector for the strongest Hg^{203} level-crossing signal. A small correction (< 2% of the linewidth) was later made in the data analysis for a residual deviation from antisymmetry with the use of the relationship given in Ref. 4. The results obtained by the two procedures are in good agreement. The first method, however, has the advantage of being simpler and of distinguishing line asymmetry, caused by $\mathrm{Im}\, A_{\mu,\mu} \neq 0$, from apparent asymmetry that may be introduced by the electronic circuitry.

The small magnetic field inhomogeneities, typically 20 and 35 mG/cm along and transverse to the magnet axis, respectively, required the cell-to-probe corrections in the magnetic field measurements discussed in Sec. III A1. The components of the cell-probe assembly and the light pipe were checked for ferromagnetic contamination with a separate proton resonance probe.

The Hg^{199} level-crossing measurements were carried out both with the natural Hg cell and with the cell containing enriched Hg^{203}. In the latter case, some of the Hg^{199} measurements were made together with the measurements of the Hg^{203} main level crossing under very similar experimental conditions. The ratio of level-crossing fields for these isotopes could be determined in this way with reduced systematic error associated with the magnetic field measurements and line asymmetry. The results of the field ratio measurements with Hg^{203} and Hg^{199} in the same cell are in good agreement with those obtained with the isotopes in separate cells.

An additional experiment was done with Hg^{199} (natural Hg cell), in which no lock-in detection was used. The measurements were done by displaying both the NMR and the amplified and filtered level-crossing signals on oscilloscopes using a sweep frequency twice that of the magnetic field modulation. The line center of the level crossing and the NMR were found as described in Sec. III A1.

The results for all the measurements of the

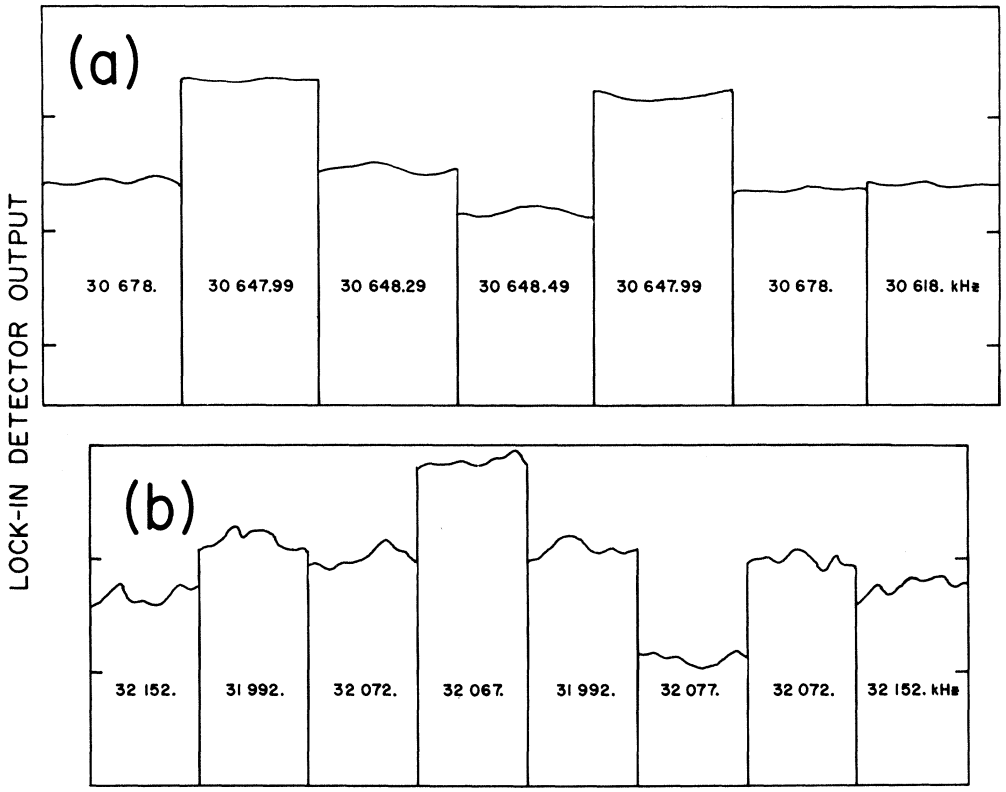

FIG. 9. Typical recorder tracings of the lock-in detector output for (a) level crossing No. 1 and for (b) level crossing No. 2, obtained by varying the magnetic field in random discrete steps. The NMR frequencies are given together with the recorder tracings for each magnetic field step. The lock-in time constant $T=30$ sec. The modulation amplitude $H_m=0.4\,\Delta H$. This amplitude gives a maximum variation of the recorder output for a magnetic field change near the line center.

level-crossing magnetic fields, given in terms of the NMR frequencies, are shown in Appendix D. The Hewlett-Packard 524B frequency counter was calibrated with the 5-MHz Natl. Bur. Std. broadcast (WWV) during the course of these measurements.

3. *Value of g_J from* Hg^{199} *Level Crossing*

The value of ν_p for Hg^{199}, given in Appendix D, was combined with the known value of the zero-field hyperfine separation $\Delta\nu$, given in Table V, to calculate g_J to high precision. An expression for g_J in terms of ν_p and $\Delta\nu$, including second-order corrections, was obtained from Eq. (15) of Ref. 20 with suitable substitutions and a change of signs to make the equation valid for a positive A. The resulting equation is

$$g_J=\frac{4\Delta\nu\,\mu_p'}{3\nu_p\mu_B}-\frac{g_I}{2}-\frac{\sqrt{6}}{6}\,\alpha[c_2(a_s-a_{1/2})-c_1\tfrac{5}{8}\sqrt{2}\,\xi a_{3/2}]\,\frac{1}{\delta_0}$$
$$+\tfrac{1}{6}\sqrt{3}\,\alpha[c_1a_s-(c_1+c_2\tfrac{5}{8}\sqrt{2}\,\xi)a_{3/2}]\,\frac{1}{\delta_2}$$
$$-\frac{\alpha^2\mu_B\nu_p}{48\mu_p'}\left(\frac{8}{\delta_0}+\frac{3\beta^2}{\delta_1}-\frac{1}{\delta_2}\right). \qquad (13)$$

α, β and c_1, c_2 are intermediate coupling coefficients for jj and LS representations, respectively. The absolute values of the energy separations between the $^3P_1$ and the $^3P_0$, $^3P_2$, and $^1P_1$ states are denoted by δ_0, δ_2, and δ_1. The quantity ξ is defined in Ref. 20 in terms of a ratio of off-diagonal to diagonal matrix elements of the magnetic dipole operator. (The analogous quantity needed for Hg^{203} calculations for the electric quadrupole operator is η.) The numerical values of the above constants associated with the $6s6p$ configuration of Hg are given in Table IV. The single-particle magnetic dipole interaction constants a_s, $a_{1/2}$, and $a_{3/2}$ and other constants in the expression for g_J specific to Hg^{199} are given in Table V.

With these constants we obtain a second-order correction of $-2.323(18)\times10^{-4}$ and the value of g_J given in Table VI. The error estimate for g_J

TABLE IV. Constants for the Hg $6s6p$ configuration used in the second-order corrections.

c_1 [a]	0.4278(22) [b]
c_2 [a]	0.9038(11) [b]
α [a]	0.9850(4) [b]
β [a]	−0.1725(24) [b]
ξ [c]	1.094
η [c]	1.354
δ_0 [d]	0.5298×10^8 MHz
δ_1 [d]	4.3939×10^8 MHz
δ_2 [d]	1.3882×10^8 MHz

[a] A. Lurio, Phys. Rev. 140, A1505 (1965).
[b] This assignment of error is ours.
[c] M. N. McDermott and W. L. Lichten, Phys. Rev. 119, 134 (1960).
[d] C. E. Moore, *Atomic Energy Levels* (U.S. GPO, Washington, D.C., 1958), Vol. III.

TABLE VI. High-precision determinations of $g_J(^3P_1)$ of Hg.

Method of measurement	g_J	Reference
High-field double resonance	1.486 094(8)	Kohler and Thaddeus [a]
Hg^{199} level crossing	1.486 110(9)	Redi and Stroke (this work)
Hg^{199} level crossing	1.486 120(16) [b]	Smith (Ref. 3)
Hg^{199} level crossing	1.486 149(10) [b]	Kaul [c]

[a] R. Kohler and P. Thaddeus, Phys. Rev. 134, A1204 (1964).
[b] Recalculated from the data using the second-order correction given in this paper.
[c] R. D. Kaul, Ph. D. thesis, Department of Physics, Case Institute of Technology, 1963 (unpublished).

includes the estimated uncertainty in the second-order correction which is assumed to be mainly due to errors in the intermediate coupling coefficients. Table VI also gives results of other g_J determinations from Hg^{199} level-crossing experiments of comparable precision and the value obtained from a precision high-field double-resonance experiment with the even isotopes. The fourth value in the table displays the only definite but unaccounted discrepancy. It may be significant that all the g_J values obtained from level-crossing experiments fall on the high side of the value obtained from the high-field double-resonance experiment. This may be due to an error in $\Delta\nu$ caused by a coherence-type frequency shift[28] which was unknown at the time this quantity was measured by a zero-field double-resonance experiment.

TABLE V. Hg^{199} constants used in the calculation of g_J. The single-electron interaction constants were calculated as described in Ref. a with c_1 and c_2 as given in Table IV and $A(^3P_1)$ obtained from $\Delta\nu$ given here.

I [b]	$\frac{1}{2}$	
Sign [b] of A	+	
$\Delta\nu$ [c]	22128.56(2)	MHz
g_I [d]	-5.423×10^{-4}	
a_s [a]	34955(45) [e]	MHz
$a_{1/2}$ [a]	5036(173) [e]	MHz
$a_{3/2}$ [a]	437(15) [e]	MHz

[a] M. N. McDermott and W. L. Lichten, Phys. Rev. 119, 134 (1960).
[b] G. H. Fuller and V. W. Cohen, in *Nuclear Data Sheets*, compiled by K. Way *et al.* (National Academy of Sciences–National Research Council, Washington, D.C., 1965), Appendix I.
[c] C. V. Stager, Phys. Rev. 132, 275 (1963).
[d] B. Cagnac, Ann. Phys. (Paris) 6, 467 (1961).
[e] Error limits represent the propagated errors from the intermediate coupling coefficients.

4. Hg^{203} *Hyperfine Structure*

In order to retain the precision of the level-crossing data needed, for example, in the hfs anomaly determination, it is necessary to include the second-order corrections in the Hg^{203} hfs analysis. This was done with the use of a modified[29] HYPERFINE-4 computer program[30] which fits the hyperfine interaction constants to the data by a least-square minimization procedure. The modification of the program consists of the replacement of the matrix of the Hamiltonian (9) by a new matrix of the same dimensionality with elements modified according to the procedure described in Sec. II B.

First, a calculation of the hyperfine interaction constants A' and B' was done by deleting the second-order correction terms from the computer program. The value of A' obtained (see Table III) was sufficiently accurate for the calculation of the Hg^{203} single-particle interaction constants a_s, $a_{1/2}$, and $a_{3/2}$ from the corresponding quantities for Hg^{199}. This was done by assuming an approximate proportionality between the single-particle constants and the A value. The approximation here, as in the calculation of $g_I(Hg^{203})$ from $g_I(Hg^{199})$ with the Fermi-Segrè formula,[21] is the neglect of the unknown hfs anomaly. Similarly, B' was sufficiently accurate for the calculation of the single-particle electric quadrupole interaction constant $b_{3/2}$ using Eq. (13) of Ref. 20. The pertinent constants for Hg^{203} used in the calculations of the second-order corrections are given in Table VII.

The corrected hfs constants A and B given in Table VIII were calculated with the use of the value of g_J obtained in this work. This table also gives the predicted zero-field hyperfine separations calculated with the same computer program.

TABLE VII. Hg^{203} constants used in the hyperfine-structure calculations.

I [a]	$\frac{5}{2}$	
Sign [a] of A	+	
g_I [b]	$-1.835(18)\times10^{-4}$	
a_s [c]	$1.183(3)\times10^4$	MHz
$a_{1/2}$ [c]	$1.70(7)\times10^3$	MHz
$a_{3/2}$ [c]	$1.48(7)\times10^2$	MHz
$b_{3/2}$	3.9×10^2	MHz

[a]Reference 7.

[b]Calculated from $g_I(Hg^{199})$ with the Fermi-Segrè formula. The error limits allow for a Hg^{199}-Hg^{203} hfs anomaly of ±1%.

[c]Error limits allow for a Hg^{199}-Hg^{203} hfs anomaly of ±1% and the propagated error from the Hg^{199} single-particle interaction constants. The relationship between the hfs anomaly, expressed in terms of the $^3P_1$ A values, and the corresponding quantity for the individual-particle constants is given in C. V. Stager [Phys. Rev. 132, 275 (1963)].

The error estimates for A and B were made by adding the following contributions: First, the error in the measurements of the level-crossing magnetic fields for Hg^{203} and Hg^{199} and in the measurement of $\Delta\nu$ of Hg^{199} gave a contribution of ±0.015 and ±0.1 MHz for A and B, respectively. (The systematic errors in the measurement of the main crossings of Hg^{203} and Hg^{199} were ignored here since the ratio of the level-crossing fields is involved.) Second, the error in the calculation of the second-order corrections arising from the uncertainty in intermediate coupling coefficients gave a contribution of ±0.006 and ±0.07 MHz. Third, the error in the calculation of the second-order corrections and the g_I term arising from a Hg^{199} – Hg^{203} hyperfine anomaly of ±1% gave a contribution of ±0.005 and ±0.11 MHz.

The quantity which was obtained most directly from the level-crossing data is $A(Hg^{203})/A(Hg^{199})$. All of the sources of error mentioned above, except the error in $\Delta\nu$, also enter in the determination of this ratio.

IV. DISCUSSION

The considerable improvement in the precision of the measurements of the hfs interaction constants that we obtained here over our previous optical spectroscopic results allows the determination of the quadrupole moment and provides a basis for obtaining the hfs anomaly. An improvement in the value of the magnetic moment is also obtained. The nuclear magnetic moment and hfs anomaly will be discussed in the light of the nuclear shell model with configuration mixing. As is discussed below, Hg^{203} is of particular interest for hfs anomaly studies because of the value of its spin. In general, the model predicts rather poorly the electric quadrupole moments. However, the results of a systematic study by Sharon[31] of the signs of the quadrupole moments of nuclei predict correctly the sign of Q of Hg^{203}.

The nuclear configuration-mixing model of Arima, Horie, and Noya[32] allows admixtures to the single-particle wave function, in which all the even nucleons are paired to zero angular momentum, of configurations in which pairs of nucleons are broken. These configurations can then contribute to deviations from the Schmidt-limit values of the nuclear magnetic dipole moments. The allowed excitations of nucleons that contribute to the nuclear moment are from orbits $j_1=l_1+\frac{1}{2}$ to $j_2=l_1-\frac{1}{2}$, in both of which there are initially even numbers of nucleons n_1 and n_2. Also allowed are excitations in and out of the odd group if $j=l_1-\frac{1}{2}$ and $j=l_1+\frac{1}{2}$, respectively. If $n_1\leq 2j_1+1$, $n_2=0$, the zeroth-order state of the nucleons is characterized by $(j_1)^{n_1}$, and if $n_1=2j_1+1$, $n_2\leq 2j_2+1$, it is characterized by $(j_2)^{n_2}$. An analogous notation is used for the nucleons that involve the odd group. It is to be noted that the admixture coefficients which enter into both nuclear-moment and hfs anomaly evaluations are calculated with a δ-function interaction for which configuration-admixture contributions are identically zero if the odd nucleon is in a $p_{1/2}$ orbit. This does not result in great disagreement between the experimental and predicted values (Schmidt limits) for these nuclei. For hfs anomalies, on the other hand, the vanishing of the admixture coefficients leads to predictions in significant disagreement with experiment. For example, such a calculation would give a value of about 10% for the hfs anomaly for the isotope pair Hg^{199}-Hg^{201}, compared to the experimental result of approximately 0.2%. Although a semiphenomenological approach[4,33] has been used to account for the nuclear magnetic moments and hfs anomalies of the

TABLE VIII. Hg^{203} results.

A	4991.35(3) MHz
B	−249.2(3) MHz
$\Delta\nu_{7/2-5/2}$	17204.5(4) MHz
$\Delta\nu_{5/2-3/2}$	12855.8(5) MHz
(μ)uncorrected [a]	$0.842(8)\mu_N$
μ [a,b]	$0.856(9)\mu_N$
Q [c]	0.46(4) b
$A(Hg^{203})/A(Hg^{199})$	0.338 301(2)

[a]Calculated from g_I given in Table VII.

[b]Diamagnetic correction has been applied using the results of F. D. Felock and W. R. Johnson [Phys. Rev. Letters 21, 785 (1968)].

[c]Calculated from B using Q/B given in Ref. 1. The Sternheimer correction is not included.

$I=\frac{1}{2}$ isotopes Hg^{195}, Hg^{197}, Hg^{199}, and Hg^{201} ($I=\frac{3}{2}$), a direct application of the theory is clearly desirable. This can be done for the pair Hg^{201}-Hg^{203}. The experimental ratios of the Hg^{201}-Hg^{199} interaction constants and nuclear moments can then be used in further analysis.

On the basis of the shell model, and considering pairing energy, the two protons in Hg that miss from completing the 82 shell are expected to be in the $3s_{1/2}$ orbit. Thus the proton contributions to the configuration-mixing effects are characterized by $(1h_{11/2})^{12}$. For the neutrons in Hg^{201} there is some ambiguity of choice: $3p_{3/2}(1i_{13/2})^{14}$ or $(3p_{3/2})^3(1i_{13/2})^{12}$. We adopt the latter which is used in the calculations of Arima, Horie, and Noya. For the Hg^{203} neutrons we have the contributions $(2f_{5/2})^5(3p_{3/2})^4(1i_{13/2})^{14}$. With the use of their parameters (with interaction strength G = 30 MeV), we obtain $\mu(Hg^{201}) = -0.48\ \mu_N$ and $\mu(Hg^{203}) = 0.89\ \mu_N$. This is to be compared to the experimental results -0.56 and $0.86\ \mu_N$.

The effect ϵ of distributed nuclear magnetization on the hfs interaction constant A is expressed by writing $A = A_{pt}(1+\epsilon)$, where A_{pt} and A describe the hypothetical point nucleus and actual cases. (There is also a relatively small extended nuclear charge distribution effect.) A_{pt} is not calculable very accurately because of the lack of precise electron wave functions. In a comparison for two isotopes, 1 and 2, we form the ratio A_1/A_2. We can approximate adequately $(A_1/A_2)_{pt}$ by g_1/g_2, where g is the nuclear g factor. Hence, we find

$$A_1/A_2 = (g_1/g_2)(1+\epsilon_1)/(1+\epsilon_2) \approx (g_1/g_2) \times (1+\epsilon_1-\epsilon_2) = (g_1/g_2)(1+{}^1\Delta^2) \ .$$

The quantity ${}^1\Delta^2$ is called the hfs anomaly. With the configurations and parameters used in the magnetic dipole moment calculations we calculate $\epsilon^{201} = -2.03\%$ and $\epsilon^{203} = -2.77\%$. From this we find ${}^{203}\Delta^{201} = -0.74\%$. A precision determination of both A factors and g values is required to determine Δ. With the use of the experimental result ${}^{201}\Delta^{199} = -0.175\%$ we calculate therefore ${}^{203}\Delta^{199} = -0.91\%$. At present, this value of Δ gives an estimate of the accuracy of our determination of the nuclear moment of Hg^{203}. Its measurement may shed light on the appropriate choice of nuclear configurations in these isotopes.

ACKNOWLEDGMENTS

We are grateful to the late Professor Francis Bitter for his interest and support of the mercury hfs studies. One of us (O.R.) would like to thank Professor D.R. Hamilton for his encouragement. We are indebted to Dr. J. Lerner of Argonne National Laboratory for performing the isotope separation. Professor W.W. Smith and Professor E.A. Phillips contributed valuable help on the computer work. Some of the computer calculations were performed at the Princeton University IBM 7094 computer which is supported by the National Science Foundation Grant No. NSF-GP 579.

APPENDIX A: $A_{\mu\mu'}$ FOR $\Delta\mu = 1$ LEVEL CROSSINGS WITH POLARIZATION-INSENSITIVE DETECTION

An explicit expression will now be given which shows that with the geometrical arrangement and light polarization used in the experiment, $\Delta\mu = 1$ level crossings are not observable. This is of importance in the identification of the detected level crossings.

With the same definitions of the geometry and polarization vectors and quantum numbers as were used in obtaining (7), we obtain for the case $\mu = m_F + 1$, $\mu' = m_F$

$$\begin{aligned} A_{\mu\mu'}(\mu > \mu') = A_{m_F+1,\,m_F} = \{ & [|\langle \alpha, m_F+1 | r_1 | \gamma, m_F\rangle|^2 |\langle \alpha', m_F | r_0 | \gamma, m_F\rangle|^2] \\ & \times (|f_b|^2 \sin\theta\cos\theta - i f_a f_b^* \sin\theta) + [|\langle \alpha', m_F | r_{-1} | \gamma, m_F+1\rangle|^2 |\langle \alpha, m_F+1 | r_0 | \gamma, m_F+1\rangle|^2] \\ & \times (|f_b|^2 \sin\theta\cos\theta - i f_a^* f_b \sin\theta) - [\langle \alpha, m_F+1 | r_0 | \gamma, m_F+1\rangle \langle \alpha', m_F | r_{-1} | \gamma, m_F+1\rangle \\ & \times \langle \alpha', m_F | r_0 | \gamma, m_F\rangle \langle \alpha, m_F+1 | r_1 | \gamma, m_F\rangle] \\ & \times [2|f_b|^2 \sin\theta\cos\theta - i(f_a f_b^* + f_a^* f_b)\sin\theta]\} (2\pi/15)^{1/2} Y_2^1(\theta', \varphi') \ . \end{aligned} \tag{A1}$$

For the arrangement used in the experiment $\theta = \theta' = \varphi' = 90^\circ$, $f_a = 1$, $f_b = 0$, the value of $A_{\mu\mu'}$ is seen to be zero.

APPENDIX B: SIGNAL STRENGTH CALCULATION

Because of a discrepancy in the published value[34] of the theoretical level-crossing signal strength for $I=\frac{1}{2}$, caused by an inconsistency in the phase convention associated with the order of I and J in a matrix element, we present a calculation in a

different representation (m_I, m_J) that is not susceptible to phase-factor errors. This is also the method for obtaining the results given in Table II for Hg^{203}. The calculation is done for the crossing of the $F=\frac{3}{2}$, $m_F=-\frac{3}{2}$ and "F"$=\frac{1}{2}$, $m_F=\frac{1}{2}$ levels, neglecting the small g_I term in the Hamiltonian. In the m_I, m_J representation, the matrix elements of the Hamiltonian

$$\mathcal{H}=\mu_B g_J H J_z + A\vec{\mathrm{I}}\cdot\vec{\mathrm{J}}$$

for $m_F=\frac{1}{2}$ are

$$\langle m_I=\tfrac{1}{2},\ m_J=0\,|\mathcal{H}|\,m_I=\tfrac{1}{2},\ m_J=0\rangle=0\ ,$$
$$\langle -\tfrac{1}{2},1\,|\mathcal{H}|\,-\tfrac{1}{2},\ 1\rangle=\mu_B g_J H-\tfrac{1}{2}A\ ,$$
$$\langle -\tfrac{1}{2},1\,|\mathcal{H}|\,\tfrac{1}{2},0\rangle=\langle\tfrac{1}{2},0\,|\mathcal{H}|\,-\tfrac{1}{2},1\rangle=\tfrac{1}{2}\sqrt{2}A\ .$$

As shown in Appendix C, the level crossing occurs at $H_c=A/\mu_B g_J$, and with an energy eigenvalue $-\frac{1}{2}A$. For the crossing levels the corresponding eigenvectors are

$$|\,^3P_1,\ \text{“}F\text{”}=\tfrac{1}{2},\ m_F=\tfrac{1}{2}\rangle = -\sqrt{\tfrac{2}{3}}\,|m_I=\tfrac{1}{2},\ m_J=0\rangle+\sqrt{\tfrac{1}{3}}\,|\,-\tfrac{1}{2},\ 1\rangle\ , \quad \text{(B1)}$$

$$|\,^3P_1,\ F=\tfrac{3}{2},\ m_F=-\tfrac{3}{2}\rangle=|\,\tfrac{1}{2},\ -1\rangle\ .$$

Hence the matrix elements needed for $A_{\mu\mu'}$ are

$$\langle{}^3P_1,\ \tfrac{3}{2},\ -\tfrac{3}{2}\,|\,r_{-1}\,|\,{}^1S_0,\ \tfrac{1}{2},\ -\tfrac{1}{2}\rangle=C\ ,$$
$$\langle{}^3P_1,\ \tfrac{1}{2},\ \tfrac{1}{2}\,|\,r_1\,|\,{}^1S_0,\ \tfrac{1}{2},\ -\tfrac{1}{2}\rangle=C/\sqrt{3}\ , \quad \text{(B2)}$$
$$\langle{}^3P_1,\ \tfrac{1}{2},\ \tfrac{1}{2}\,|\,r_0\,|\,{}^1S_0,\ \tfrac{1}{2},\tfrac{1}{2}\rangle=-\sqrt{2}\,C/\sqrt{3}\ ,$$

where

$$C\equiv\langle{}^3P_1\|r\|\,{}^1S_0\rangle\,|/\sqrt{3}\ .$$

With the geometry and polarization vectors defined in Sec. IIA we find

$$A_{1/2,\,-3/2}=C^4(\tfrac{1}{12})[\,|f_a|^2-|f_b|^2\cos^2\theta + i(f_a f_b^*+f_a^* f_b)\cos\theta]\sin^2\theta' e^{+i2\varphi'}. \quad \text{(B3)}$$

For $\theta=\theta'=\varphi'=90^\circ$, $f_a=1$, $f_b=0$ this becomes $A_{1/2,\,-3/2}=-C^4(\frac{1}{12})$. The background term R_0 is calculated under the assumption that the incident light excites within its Doppler width only the two levels involved in the crossing. We thus find $R_0=\frac{7}{18}C^4$. Hence we obtain the result $(A_{\mu\mu'}+A_{\mu\mu'}{}^*)/R_0=-0.43$.

APPENDIX C

1. Analytic Expressions for Level-Crossing Magnetic Field and Energy Values for $J=1$, $B=0$

It is possible to obtain simple analytic expressions for the magnetic field value and the energy at which the levels cross in the case of $J=1$ and arbitrary I if the quadrupole interaction is zero and we neglect the small g_I term in the Hamiltonian. The analytic approach exhibits the simple feature that all the nonzero-field level crossings coincide. The Hamiltonian $\mathcal{H}=A\vec{\mathrm{I}}\cdot\vec{\mathrm{J}}+xJ_z$, where $x\equiv\mu_B g_J H$. The m_F submatrices of $\mathcal{H}$ are of order 3 if $|m_F|<I$, 2 if $|m_F|=I$, and 1 if $|m_F|=I+1$. The corresponding secular equations for the energy eigenvalues σ are

$$\sigma^3+2A\sigma^2-[A^2I(I+1)+x^2+2Am_F x-A^2]\sigma - A^3I(I+1)-A^2m_F x=0\ , \quad \text{(C1)}$$
$$\sigma^2-[A(I-1)\pm x]\sigma-IA^2=0 \quad (m_F=\pm I)\ , \quad \text{(C2)}$$
$$\sigma-(IA\pm x)=0 \quad [m_F=\pm(I+1)]\ . \quad \text{(C3)}$$

Level crossings occur at values of x_c for which polynomials that correspond to different m_F have coincident roots σ_c. Such values of x_c can be found with the use of the following theorem[35]:

Let

$$u(y)=a_0y^n+a_1y^{n-1}+\cdots+a_{n-1}y+a_n\ ,$$
$$v(y)=b_0y^s+b_1y^{s-1}+\cdots+b_{s-1}y+b_s\ ,$$

then $u(y)$ and $v(y)$ have at least one common root if and only if

$$\left|\begin{array}{l}
\left.\begin{array}{l} a_0a_1\cdots\cdots a_n\,0\,0\cdots 0 \\ 0\,a_0a_1\cdots\cdots a_n0\cdots 0 \\ \cdot \\ \cdot \\ \cdot \\ 0\cdots 0\,0a_0a_1\cdots\cdots a_n \end{array}\right\} s\text{ rows} \\
\left.\begin{array}{l} b_0b_1\cdots b_s\,0\,0\cdots\cdots 0 \\ 0\,b_0b_1\cdots b_s\,0\cdots\cdots 0 \\ \cdot \\ \cdot \\ \cdot \\ 0\cdots\cdots 0\,0b_0b_1\cdots b_s \end{array}\right\} n\text{ rows}
\end{array}\right| = 0\ .$$

We consider this theorem for the case of two polynomials of degree 3 in σ, for which $a_0=b_0=1$ and $a_1=b_1=p$. The determinant equation becomes

$$(b_3-a_3)^3-(b_2-a_2)[\,p(b_3-a_3)^2+a_3(b_2-a_2)^2 - a_2(b_2-a_2)(b_3-a_3)]=0\ . \quad \text{(C4)}$$

If we apply (C4) to the secular equations (C1) for any pair of levels m_F and m_F' ($|m_F|<I$), we obtain

$$4A^4(m_F-m_F')^3x^3[x-(\tfrac{1}{2}A)(2I+1)]\,[x+(\tfrac{1}{2}A)(2I+1)]=0\ . \quad \text{(C5)}$$

The crossing field $H_c\neq 0$ is thus given by

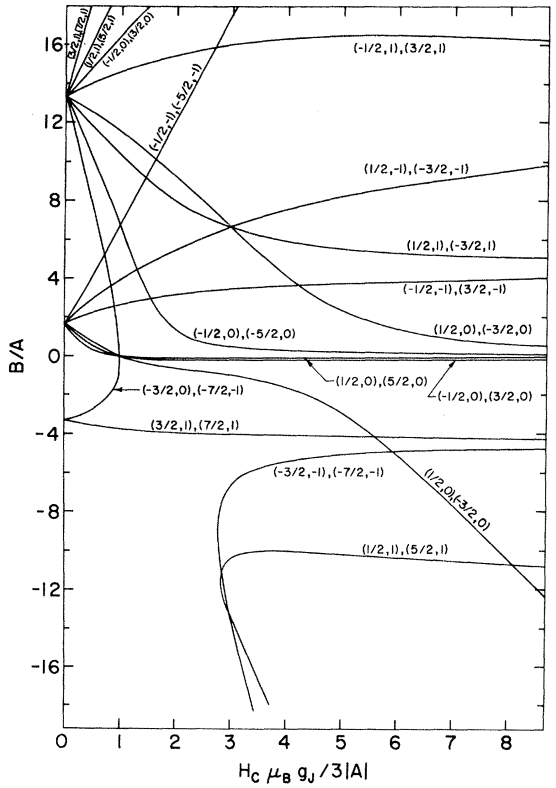

FIG. 10. The relationship, for $I=\frac{5}{2}$, between B/A and the level-crossing magnetic field values H_c given in units of $3|A|/\mu_B g_J$. The given labels (m_F, "m_J"), (m_F', "m_J'") are for $A>0$. A diagram for $A<0$ can be obtained by changing the signs of m_F and "m_J".

$$x_c=(\tfrac{1}{2}|A|)(2I+1) \ . \tag{C6}$$

With this value x_c the secular equations (C1) become

$$(\sigma+\tfrac{1}{2}A)\left[\sigma^2+\tfrac{3}{2}A\sigma-2A^2I(I+1)-A|A|m_F(2I+1)\right]=0 \ ,$$

which gives an energy (measured from the "center of gravity")

$$\sigma_c=-\tfrac{1}{2}A \tag{C7}$$

common to all the crossing m_F levels. Hence there are $2I-1$ m_F levels with $|m_F|<I$ that cross at a single value of σ and x.

If we apply the theorem also to pairs of equations which include (C2) and (C3), we find additional crossings which also occur at the energy and field values given by (C6) and (C7). The levels involved are $m_F=-(I+1)$ and I for $A>0$ and $m_F=I+1$ and $-I$ for $A<0$. Thus for $B=0$ there is but one crossing which involves $2I+1$ levels.

2. Dependence of Level-Crossing Fields on B/A for $J=1$, $I=\frac{5}{2}$

For $B\neq 0$, a numerical calculation was done to determine the level-crossing fields as a function of B/A. Instead of first obtaining the energy-versus-magnetic-field diagram and then looking for the level crossings, it is more straightforward to solve (C4) [or analogous equations if (C2) or (C3) are involved] for the crossing magnetic field parameters x_c. This method was used to obtain the results shown in Fig. 10. An enlargement of the region for small B/A is shown in Fig. 5.

APPENDIX D: DETAILED PRESENTATION OF EXPERIMENTAL DATA

The Hg^{203} and Hg^{199} level-crossing data are shown in Table IX. The uncertainties given represent three times the standard deviation of the mean plus the estimated systematic errors associated with the magnetic field measurements and line asymmetry. The measurement of ν_p for Hg^{199} and Hg^{203} (No. 1) with the isotopes in the same cell and other conditions as nearly identical as possible gives $\nu_p(Hg^{203})/\nu_p(Hg^{199})=1.014\,911(2)$. This value is in agreement with the ratio of the average values of $\nu_p(Hg^{203})$ and $\nu_p(Hg^{199})$ given in Table IX.

TABLE IX. Hg^{203} and Hg^{199} level-crossing data.

Isotope and crossing No.	Mean NMR frequency ν_p (kHz)	No. of determinations	Weighted mean of all data (kHz)	Remarks
Hg^{203} (1)	30 648.29(20)	6		Field-sweep method
	30 648.30(14)	3		Point-by-point method
	30 648.42(10)	3		Point-by-point method, line asymmetry correction by field reversal
Hg^{203} (1)			30 648.37(15)	
Hg^{203} (2)	32 071.5(15)	4		Field-sweep method
	32 072.2(7)	12		Point-by-point method
Hg^{203} (2)			32 072.1(11)	
Hg^{203} (3)	33 725.7(20)	6		Field-sweep method
	33 724.9(15)	11		Point-by-point method
Hg^{203} (3)			33 725.2(18)	
Hg^{203} (4)	36 430. (25)	3		Field-sweep method
Hg^{203} (4)			36 430. (25)	
Hg^{199}	30 198.05(14)[a]	2		Point-by-point method
	30 198.15(10)[b]	3		Point-by-point method, line asymmetry correction by field reversal
	30 198.14(15)[c]	53		Observations made without lock-in detection system
Hg^{199}			30 198.12(13)	

[a]All determinations made with the cell containing Hg^{203}.

[b]Two determinations made with the natural Hg cell, the other as in Ref. a.

[c]All determinations made with the natural Hg cell.

†Work supported by the U.S. Atomic Energy Comm. and the Higgins Scientific Trust Fund at Princeton University, and by the National Science Foundation at New York University. A portion of this work was done at MIT with support from the U.S. Army Signal Corps, the Air Force Office of Scientific Research, and the Office of Naval Research.

††On leave Sept. 1969–Sept. 1970 at the Laboratoire Aimé Cotton, C.N.R.S. II, Faculté des Sciences, Orsay, France.

[1]W. J. Tomlinson, III and H. H. Stroke, Nucl. Phys. 60, 614 (1964).

[2]F. Bitter, Appl. Opt. 1, 1 (1962).

[3]S. P. Davis, T. Aung, and H. Kleiman, Phys. Rev. 147, 861 (1966).

[4]W. W. Smith, Phys. Rev. 137, A330 (1965) (Hg^{193*}, Hg^{195*}, and Hg^{195} level-crossing experiments).

[5]O. Redi and H. H. Stroke, Bull. Am. Phys. Soc. 10, 456 (1965) (more recent level-crossing results for Hg^{193*} and main level-crossing determination for Hg^{193}).

[6]J. C. Lehmann and R. Barbé, Compt. Rend. 257, 3152 (1963).

[7]O. Redi and H. H. Stroke, Phys. Letters 8, 257 (1964).

[8]O. Redi and H. H. Stroke (unpublished).

[9]F. D. Colegrove, P. A. Franken, R. R. Lewis, and R. H. Sands, Phys. Rev. Letters 3, 420 (1959).

[10]H.R. Hirsch, Bull. Am. Phys. Soc. 5, 274 (1960).

[11]H. H. Stroke, G. Fulop, S. Klepner, and O. Redi, Phys. Rev. Letters 21, 61 (1968).

[12]V. F. Weisskopf, Ann. Physik 9, 23 (1931).

[13]G. Breit, Rev. Mod. Phys. 5, 91 (1933).

[14]P. A. Franken, Phys. Rev. 121, 508 (1956).

[15]M. E. Rose and R. L. Carovillano, Phys. Rev. 122, 1185 (1961).

[16]K. E. Lassila, Phys. Rev. 135, A1218 (1964).

[17]H. Wieder and T.G. Eck, Phys. Rev. 153, 103 (1967).

[18]Note that in Ref. 11 the coordinate system is chosen so that the x component of $\vec{k}_i$ is *negative*. This different definition results in a different expression for $A_{\mu\mu'}$, written in terms of $\vec{k}_i$, $\vec{k}_s$, and $\vec{f}$. The physical results are, of course, the same regardless of the initial arbitrary definition.

[19]C. Schwartz, Phys. Rev. 97, 380 (1955).

[20]A. Lurio, M. Mandel, and R. Novick, Phys. Rev. 126, 1758 (1962).

[21]N. F. Ramsey, *Molecular Beams* (Oxford U.P., Oxford, England, 1956).

[22]C. P. Slichter, *Principles of Magnetic Resonance* (Harper and Row, New York, 1963), pp. 231–235.

[23]M. Schein, Helv. Phys. Acta Suppl. 2, 1 (1929).

[24]B. V. Rollin, Rept. Progr. Phys. 12, 22 (1949).

[25]E.R. Andrew, *Nuclear Magnetic Resonance* (Cambridge U.P., Cambridge, England, 1958); W. C. Dickinson, Phys. Rev. 81, 717 (1951).

[26]E. Klein, Z. Physik 208, 28 (1968).

[27]J. Lerner (private communication).

[28]C. J. Schuler, Ph.D. thesis, Department of Physics, Massachusetts Institute of Technology, 1964 (unpublished). A. Omont, Compt. Rend. 258. 1193 (1964).

[29]The modifications to include the $^3P_2$ and $^3P_0$ state perturbations were made by P. Thaddeus. We have made a further modification to include the perturbations due to the $^1P_1$ state.

[30]We are grateful to Howard Shugart for making the original version of this program available to us. A description of this program is found in H. L. Garvin, T. M. Green, E. Lipworth, and W. A. Nierenberg, Phys. Rev. 116, 393 (1959).

[31]Y. Y. Sharon, Nucl. Phys. A99, 321 (1967).

[32]H. Noya, A. Arima, and H. Horie, Progr. Theoret. Phys. (Kyoto) Suppl. 8, 33 (1958).

[33]H. H. Stroke, R. J. Blin-Stoyle, and V. Jaccarino, Phys. Rev. 123, 1326 (1961).

[34]H. R. Hirsch, J. Opt. Soc. Am. 51, 1192 (1961).

[35]S. Borofsky, *Elementary Theory of Equations* (MacMillan, New York, 1950).